

Synthesis and Characterization of Photocatalyst Nanocomposite for the Degradation of Organic Pollutants in Wastewater

Ratnawulan^{1*}, Detty Rahmadhani¹, Ahmad Fauzi¹, Riri Jonuarti¹,
Faridah Lisa Supian², Fadhila Ulfa Jhora¹

¹ Research Center for Theoretical and Experimental of Functional Materials, Department of Physics, Faculty of Mathematics and Natural Sciences, Universitas Negeri Padang, Jalan. Prof Hamka, Padang 25131, West Sumatera, Indonesia

² Department of Physics, Faculty of Sciences and Mathematics, University Pendidikan Sultan Idris, Tanjung Malim, Perak 35950, Malaysia

* Corresponding author's email: ratnawulan@fmipa.unp.ac.id

ABSTRACT

Various efforts can be made to obtain clean water in the environment by utilizing semiconductor technology. This study aims to inform the synthesis and characterization of $\text{MnO}_2/\text{CuO}/\text{Fe}_2\text{O}_3$ photocatalyst for crystal violet degradation in wastewater. Nanocomposite was synthesized through a sol-gel process with three semiconductor materials doped. X-ray diffraction (XRD) was employed to analyze the nanocomposite structure and determine crystal size. Fourier transform infrared (FTIR) was used to provide functional groups in the nanocomposite. A scanning electron microscope (SEM) can characterize surface morphology and particle size. The results of the SEM show that an increase in sintering temperature causes the smallest particle sizes to be 54.79 nm. The result of characterization using the ultraviolet-visible (Uv-Vis) spectrophotometry analysis the most effective band gap value in photocatalyst activity was 1.36 eV. The optimum percent of degradation $\text{MnO}_2/\text{CuO}/\text{Fe}_2\text{O}_3$ catalyst was 50.40% for the sample at a temperature of 400 °C under irradiation with sunlight for six hours. Test results show that increased sintering temperature increased the photocatalytic activity.

Keywords: photocatalyst, temperature, band gap energy, degradation, wastewater.

INTRODUCTION

Water pollution has resulted in numerous environmental issues. Most of these sectors dump toxic waste such as oxidizing agents (bleach) into fresh water that flows without preliminary treatment (Touqeer et al., 2020). These organic contaminants can reduce water quality and endanger human life (Gayatri et al., 2021). Among the many potential solutions to this problem, photocatalysis is especially promising because it is economical, non-toxic, safe, and renewable. In photocatalytic processes, sunlight can be used as an energy source to degrade organic contaminants using semiconductor materials (Sukma et al., 2019).

Many studies increase photocatalytic activity by using semiconductor oxides or combining

several materials and semiconductor oxides such as iron oxide (Ratnawulan et al., 2022). As a result of its environmentally friendly properties, low catalyst costs, nontoxicity, high specific area, and high crystallinity. Hematite (Fe_2O_3) exhibits promising photocatalytic activity n-type semiconductor metal oxide, influenced by particle size, and has an optical band gap of ~2.1 eV (Amin et al., 2016; Alp et al., 2019). In addition, these oxide particles coagulate easily in fallow solutions, decreasing photocatalytic efficiency. Therefore, a special strategy is needed for the use of iron oxide catalysts (Touqeer et al., 2020; Alagiri & Hamid, 2015).

One solution was to apply the doping with oxides that can be easily dispersed in an organic medium and homogeneously loaded onto the supporting material as copper oxide (CuO) with a

band gap of ~ 1.2 eV (Alp et al., 2019; Mesrar et al., 2023). Previous studies have successfully synthesized photocatalyst nanocomposite layers supported by different semiconductor oxides, including CuO/Fe₂O₃/Polystyrene. The composite has proven successful in reducing catalyst particle size, but the photocatalytic activity was still very low regarding pollutant degradation was 0.24% and the energy gap was 3.1 eV (Ratnawulan et al., 2021).

Various types of metal-based oxides, such as TiO₂, RuO₂, MnO₂, NiO, and CO₃O₄, are synthesized in the laboratory (Karimi et al., 2019). Manganese dioxide can be used to protect the environment and degrade organic contaminants in wastewater. MnO₂, part of a new generation of environmentally friendly catalysts, was a promising material for heterogeneous photocatalysts, with an energy band gap of ~ 1 eV (Chiam et al., 2020). Nanostructured manganese dioxide was the best material for this application due to its natural abundance and non-toxicity (Pawar et al., 2019; Mondal et al., 2019).

Based on these advantages, MnO₂ semiconductors were selected as supporting components for the development of a thin-film MnO₂/CuO/Fe₂O₃ photocatalyst nanocomposite to increase the degradation activity of organic contaminants. This approach, in addition to reducing the energy band gap so photocatalyst activity that is maintained under sunlight, is cost-effective, eco-friendly, and non-toxic (Yuniar et al., 2023). Therefore, MnO₂/CuO/Fe₂O₃ materials have a promising application in decomposing pollutants. Various catalysts have been developed for this purpose, some of which are homogeneous, heterogeneous, and hybrid (Mamiyev & Balayeva, 2022). This article describes the synthesis and photo characterization of MnO₂/CuO/Fe₂O₃ nanocomposite, sintered at different temperatures to obtain the preparation catalyst at which optimum degradation is achieved.

EXPERIMENTAL

Material and Methods

The semiconductor materials for photocatalyst synthesis used in this research were MnO₂, CuO, and Fe₂O₃. These materials were obtained commercially. Fe₂O₃ and CuO powders were obtained from Merck Loba, and MnO₂ powders were obtained from PUDAK. Other ingredients

included crystal violet (C₂₅N₃H₃₀Cl), ethylene glycol (C₂H₆O₂), nitric acid (HNO₃), acetic acid (CH₃COOH), ethanol (C₂H₅OH), and distilled water, which were obtained commercially from PT. Brataco, Bandung, Indonesia.

Synthesis of MnO₂/CuO/Fe₂O₃ nanocomposite

The powder was ground using a 3D High-Energy Milling technique called HEM-3D. MnO₂ and CuO powders were ground for 20 hours, and Fe₂O₃ powder was ground for five hours (Sukma et al., 2019; Ratnawulan et al., 2022; Anisa et al., 2023). Furthermore, the process of making MnO₂/CuO/Fe₂O₃ composites was carried out through sol-gel technique with composition at a ratio of 0.8:3:1 (Azleen et al., 2023). To make precursor Fe(NO₃)₂·9H₂O, 1.25 grams of Fe₂O₃ were mixed with 0.18 grams of (nitric acid) HNO₃. To make the precursor Cu(CH₃COO)₂·H₂O, 3.7 grams of CuO were mixed with 0.54 grams of (acetic acid) CH₃COOH. Each precursor, Fe(NO₃)₂·9H₂O and Cu(CH₃COO)₂·H₂O, was reacted with 5 ml of ethanol at 0.3 M concentration, then stirred at room temperature (25°C) until completely mixed (Zhang et al., 2019). After 15 minutes, 1 gram of MnO₂ powder was added little by little to the precursor mixture. Then, ethylene glycol (10% of the solution composition) was added and stirred for 30 minutes to form MnO₂/CuO/Fe₂O₃ nanocomposite gel (Touqeer et al., 2020). The spin-coated process was used to create a thin layer of MnO₂/CuO/Fe₂O₃ substrate. By applying three drops of MnO₂/CuO/Fe₂O₃ nanocomposite gel to the whole glass surface. The substrate for this investigation was a 1×1 centimeter glass item. The substrate was then spun at 1000 rpm for one minute (Ratnawulan et al., 2022).

Photocatalytic experiments and characterization

MnO₂/CuO/Fe₂O₃ nanocomposites were known for their ability to degrade crystal violet color solutions via their photocatalyst activity. A total of 50 ml of CV dye solution at 10 ppm concentration and one sheet of photocatalysis film were put in a 100 ml beaker. A magnetic stirrer was used to mix the solution for 10 minutes. The solution was then dried in the sun for four hours and six hours. The value of (A₀) absorbance before and (A₁) after shall be considered when calculating the percentage of degradation (Mondal et

al., 2019). The crystal size was determined using XRD with a Philips X' Pert PRO (3040-60) diffractometer and the Scherrer equation was used to calculate the crystal size, $D = 0.9/\beta \cos\theta$ (Le et al., 2021). The percentage of crystallinity was determined using the equation $\text{Crystallinity (\%)} = (A_c / (A_c + A_a)) \times 100$ (Permana et al., 2022). Fourier transformation infrared spectroscopy (FTIR) was employed using a Perkin Elmer Frontier C90704 Spectrum IR Version 10.6.1, instrument to identify vibration modes in the functional group. The surface structure and particle measurement were utilized with SEM-type INSPECT-S50. In addition, the Analytik Jena Specord 200 Plus Uv-Vis Spectrometer was used for irradiation.

RESULTS AND DISCUSSION

X-ray diffraction analysis

In XRD analysis, peak position in diffraction patterns may identify distortions in the crystal structure and the presence of phases formed. Peak width in a diffraction pattern measured at Full Width at Half Maximum (FWHM) may be used to determine the crystal size (Wadi et al., 2020). Figure 1 illustrates the XRD pattern of the $\text{MnO}_2/\text{CuO}/\text{Fe}_2\text{O}_3$ nanocomposite at various temperatures 200°C, 250°C, 300°C, 350°C, and 400°C.

X-ray diffraction analysis was detected at a range of $2\theta = 20\text{--}80^\circ$, showing that the diffraction peak of five different coexisting phase structures, namely hematite (Fe_2O_3), copper ferrite (CuFe_2O_4), tenorite (CuO), jacobsite (MnFe_2O_4), and Fe_2O_3 ; CuO ; MnO_2 phase. The rhombohedral

crystal structure of Fe_2O_3 was confirmed in peaks at an angle of $2\theta = 24.60^\circ$ and 33.55° . The copper ferrite's tetragonal structure was confirmed in peak at an angle of $2\theta = 35.90^\circ$. The formation of the CuFe_2O_4 phase resulted from the combination of iron oxide and copper oxide. This compound follows the general formula AB_2O_4 , where A represents a metal ion with a $+2$ valence and B represents a metal ion with a $+3$ valence (Liu et al., 2020). Copper ferrite (CuFe_2O_4) possesses an inverse spinel structure, consisting of 8 Cu^{2+} ions and 16 Fe^{3+} ions within a single unit cell. The tenorite peak was identified with a monoclinic structure at angles of $2\theta = 39.11^\circ$, 49.13° , 58.61° , and 61.93° . The jacobsite peak was confirmed with a cubic structure at an angle of $2\theta = 64.37^\circ$ (Mondal et al., 2019; Ratnawulan et al., 2022). The combination of Fe_2O_3 ; CuO ; MnO_2 phase was identified at angles of $2\theta = 75.57^\circ$, 72.73° , 75.36° , 72.67° , and 72.69° . The increase in sintering temperature did not have any impact on the crystal structure of the sample. The XRD analysis reveals that the variations in sintering temperature do not alter the phase or crystal structure formed. Furthermore, the existence of clearly visible diffraction peaks indicates that this catalyst has an excellent crystal structure and can aid in the stabilization of the catalytic activity

JCPDS-ICDD#00-001-1117 for CuO , JCPDS-ICDD#01-084-0311 for Fe_2O_3 , and JCPDS-ICDD#00-001-0799 for MnO_2 were used to examine all composite diffraction peaks. Using the Scherrer equation, the crystal size was determined to be hematite: 27.63 nm. Copper Ferrite: 24.47 nm. Tenorite: 26.76 nm. Jacobsite, 23.84 nm. However, the sintering temperature affects the crystallite size of the $\text{MnO}_2/\text{CuO}/\text{Fe}_2\text{O}_3$ nanocomposite. The smallest crystal size 22.80 nm, was obtained at a temperature of 400°C. The diffraction pattern shows that this catalyst has a relatively small structure of crystals, exhibiting nanoscale characteristics with significant catalytic activity and this increases the surface area accessible for the reaction.

The optimum percentage crystallinity of the $\text{MnO}_2/\text{CuO}/\text{Fe}_2\text{O}_3$ composite was 89.22%. High crystallinity was required to prevent the recombination of electron holes and improve photocatalyst action. Crystallinity has a strong influence on photocatalysis activity in the composite. Thus, the catalyst has an excellent crystal structure, small crystal size, and high percentage crystallinity, resulting in strong catalytic efficiency.

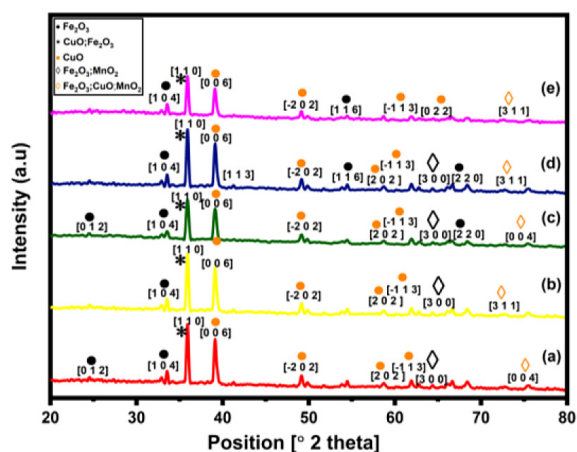


Figure 1. XRD patterns samples sintered at (a) 20°C, (b) 250°C, (c) 300°C, (d) 350°C, and (e) 400°C

Fourier transform infrared spectroscopic analysis

The presence of vibration modes and carbon groups can be seen in Figure 2 from the FTIR spectra showing the results of Fourier transform infrared (FTIR) characterization for MnO₂/CuO/Fe₂O₃ nanocomposite.

A significant peak of FTIR characterization results in nanocomposite with temperature variation in the Cu-O functional group at a wavenumber of 414.54 cm⁻¹, 416.19 cm⁻¹, 427.86 cm⁻¹, 415.02 cm⁻¹, 409.83 cm⁻¹, 460.54 cm⁻¹, 455.66 cm⁻¹, 460.18 cm⁻¹, 457.08 cm⁻¹, and 457.94 cm⁻¹. The Cu-O functional group lies in the FTIR vibrational frequency range of 400 cm⁻¹ to 600 cm⁻¹ (Aroob et al., 2023). The characteristic bands observed at 521.68 cm⁻¹, 526.01 cm⁻¹, 527.41 cm⁻¹, 534.31 cm⁻¹, and 527.22 cm⁻¹ were associated with the basic vibration mode Mn-O. The wave numbers at 768.05 cm⁻¹, 768.48 cm⁻¹, 767.63 cm⁻¹, 767.66 cm⁻¹, and 766.65 cm⁻¹ were the absorption for C-H. The functional groups C-H include ethylene glycol, nitric acid, acetic acid, ethanol, and aromatic, confirming the role of the MnO₂/CuO/Fe₂O₃ synthesis (Fardood et al., 2019). The wave number at 922.33 cm⁻¹, 922.12 cm⁻¹, 924.77 cm⁻¹, 921.08 cm⁻¹, and 922.87 cm⁻¹, the Fe-O vibration mode was discovered.

The increase in calcination temperature causes the Cu-O bond to shift towards a shorter wave number 409.83 cm⁻¹ to 460.54 cm⁻¹, and the Mn-O bond to shift to a shorter one 521.68 cm⁻¹ to 534.31 cm⁻¹. However, the Fe-O bond shifts towards a longer wave number 921.08 cm⁻¹ to 924.77 cm⁻¹. The FTIR spectra indicate that the

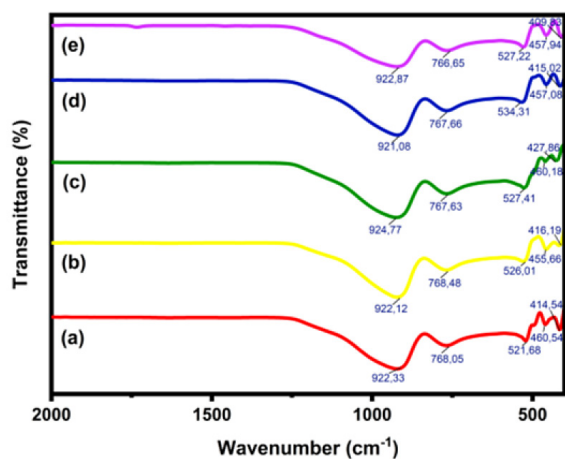


Figure 2. FTIR pattern samples sintered at (a) 200°C, (b) 250°C, (c) 300°C, (d) 350°C, and (e) 400°C

MnO₂/CuO/Fe₂O₃ material provides different absorption regions on the infrared spectra. Furthermore, the presence of functional groups from FTIR data showed that carbon atoms with hydrogen bonds (C-H) with the type of aromatic compound and absorption were observed at a wave number 766.65 cm⁻¹ to 768.48 cm⁻¹. Previous research has added this evidence by identifying the existence of the Mn-O group in the nanocomposite at wave numbers ranging from 500 cm⁻¹ to 600 cm⁻¹, and the Fe-O bonds at wave numbers ranging from 800 cm⁻¹ to 900 cm⁻¹ (Zhang et al., 2019) and (Fufa et al., 2014). The results of FTIR analyses were able to explain variations in the infrared spectrum caused by molecule adsorption on the catalyst surface. Each catalyst surface contains functional groups that form as a result of temperature changes, allowing them to interact with reactant molecules.

SEM analysis

Figure 3 illustrates the SEM analysis conducted to investigate the effect of calcination temperature on the morphology of MnO₂/CuO/Fe₂O₃ nanocomposites. The variation in sintering temperature influences particle size.

Figures 3 (a) and (b) show the SEM images of the particles were few, rougher, irregular, and agglomerated. Figure 3 (c) shows the particle morphology looked homogeneous, the resulting thin layer was evenly distributed, and less cavity. Figure 3 (d) shows that few visible particles and many cavities were found. Figure 3 (e) shows that small particles were visible and less agglomerated in SEM images at a temperature of 400°C. It has the smallest average particle size value 54.79 nm. This leads to a significant increase in surface area, making it ideal for exhibiting photocatalytic capabilities. Figure 3 (f) shows that variation in the sintering temperature of the MnO₂/CuO/Fe₂O₃ nanocomposite affects the particle size. The elevated temperature within the sintered chamber resulted in alterations to the surface structure of the particles (Wang et al., 2018).

The photocatalyst activity of composite MnO₂/CuO/Fe₂O₃ was strongly influenced by the crystallinity and size of the synthesis results. The calcination process carried out at 400°C resulted in the rearrangement of the MnO₂/CuO/Fe₂O₃ composite crystal structure and increased the percentage of composite crystallinity. The calcination process aims to form Mn-O, Cu-O, and Fe-O bonds and

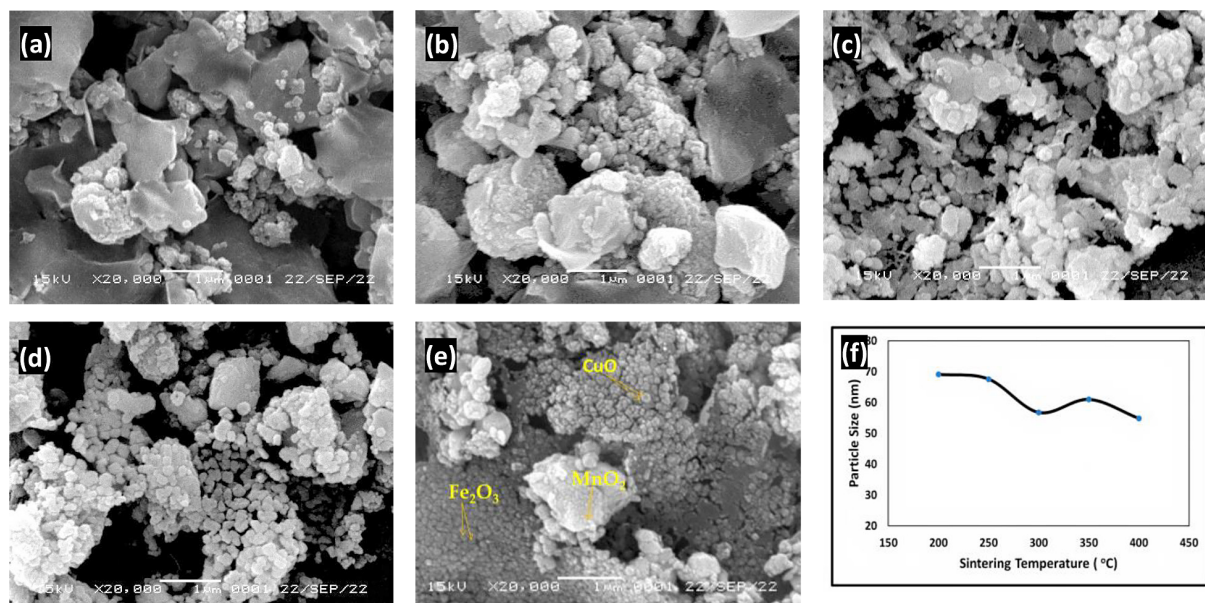


Figure 3. SEM Images Samples Sintered at (a) 200°C, (b) 250°C, (c) 300°C, (d) 350°C, and (e) 400°C (f) Affects the particle size

perfect the crystal. The composite at a calcination temperature of 400°C was the best photocatalytic activity compared to other temperatures. The effect on particle size was attributed to the fact that each phase's structure possesses a large surface area and smaller particle size. The higher the temperature of the calcination, the greater the crystallinity of the material, and the smaller the crystal size of the resulting crystals. The photocatalyst activity will increase when the particle size is smaller. Semiconductors have good photocatalytic activity if they have a nano-size crystal (Mandrekar & D'souza, 2023). From temperature variations, the synthesis of $\text{MnO}_2/\text{CuO}/\text{Fe}_2\text{O}_3$ samples obtained nano-sizes below 100 nm.

Uv-Vis spectroscopy analysis

Figure 4 illustrates the absorption spectrum of the $\text{MnO}_2/\text{CuO}/\text{Fe}_2\text{O}_3$ nanocomposite using Uv-Vis spectroscopy was plotted using Tauc's relation formula.

Figure 4 shows the result of the band gap energy which ranged from 1.36 to 1.64 eV, at temperatures of 200°C, 250°C, 300°C, 350°C, and 400°C. At the wavelength ranges of 300 to 800 nm, $\text{MnO}_2/\text{CuO}/\text{Fe}_2\text{O}_3$ photocatalyst showed a consistent absorption peak. This uptake explains the ability of $\text{MnO}_2/\text{CuO}/\text{Fe}_2\text{O}_3$ nanocomposites to act as photocatalysts that can be used for CV degradation using solar energy in a wider

spectrum, from ultraviolet to infrared. The smallest energy gap value was found at 400°C, which was 1.36 eV. The effect of temperature variation on the band gap value will decrease with an increase in the temperature used. In the research conducted, it was found that a thin layer of $\text{MnO}_2/\text{CuO}/\text{Fe}_2\text{O}_3$ nanocomposites was able to absorb almost all the sunlight spectrum to carry out photocatalyst activities.

The photocatalyst properties of this semiconductor material can reduce liquid pollutants by utilizing sunlight in visible to infrared light which is very abundant in its natural presence (Ani et al., 2018). The sintering temperature of $\text{MnO}_2/\text{CuO}/\text{Fe}_2\text{O}_3$ nanocomposites affects the energy band gap

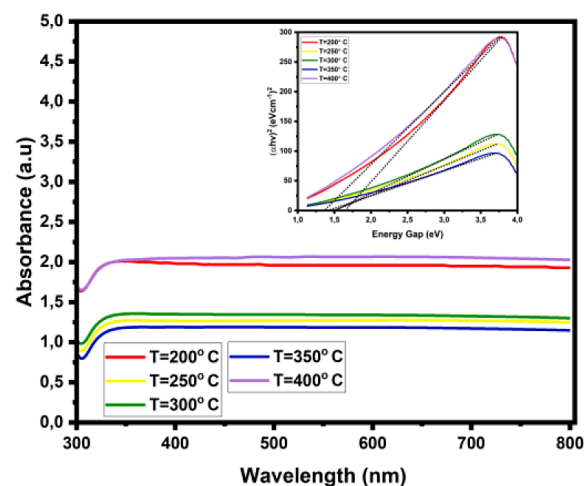


Figure 4. UV-visible absorption spectra and tauc plot

and photocatalyst activity in degrading a crystal violet solution. The pollutant degradation process can occur if the $\text{MnO}_2/\text{CuO}/\text{Fe}_2\text{O}_3$ catalyst is exposed to light greater than the catalyst's band gap energy (E_g), resulting in electron transfer.

Photocatalyst activities

Figure 5 shows the absorbance of the crystal violet solution due to the photocatalyst activity of a thin layer of $\text{MnO}_2/\text{CuO}/\text{Fe}_2\text{O}_3$ at various temperatures. The percentage degradation by the $\text{MnO}_2/\text{CuO}/\text{Fe}_2\text{O}_3$ catalyst after being exposed to sunlight for four hours and six hours. The highest photocatalyst activity was achieved at a temperature of 400°C . This was indicated by the smaller absorption achieved as compared to that obtained at other temperatures and a higher percentage of degradation than that seen at other temperatures.

In Figures 5 (a) and (b), the resulting CV degradation increased with increasing sintering temperature, after four and six hours of photodegradation of the CV solution under solar radiation.

In Figure 5 (c), after 6 hours of photodegradation of crystal violet under solar radiation, 29.72%, 32.43%, 40.54%, 43.24%, and 50.40% of the CV was degraded by $\text{MnO}_2/\text{CuO}/\text{Fe}_2\text{O}_3$ photocatalyst sintering at 200°C , 250°C , 300°C , 350°C , and 400°C , respectively. The photodegradation of CV is highly dependent on the sintering temperature of the photocatalyst. The highest CV degradation was obtained using $\text{MnO}_2/\text{CuO}/\text{Fe}_2\text{O}_3$ photocatalysts sintering at a temperature of 400°C . The increase in sintering temperature increased the pore size of $\text{MnO}_2/\text{CuO}/\text{Fe}_2\text{O}_3$ photocatalyst nanocomposites and was responsible for CV absorption before a photodegradation reaction occurred.

Figure 5 (d) shows that when the semiconductor photocatalyst experiences light energy greater than the semiconductor band, electron-hole pairs are formed due to the absorption of photon energy ($h\nu$). Sunlight improves the efficacy of catalysts in initiating photochemical reactions (Surendra et al., 2018). The $\text{MnO}_2/\text{CuO}/\text{Fe}_2\text{O}_3$ catalyst was exposed to sunlight as an energy source so that the transfer of electrons occurs, resulting in reduced

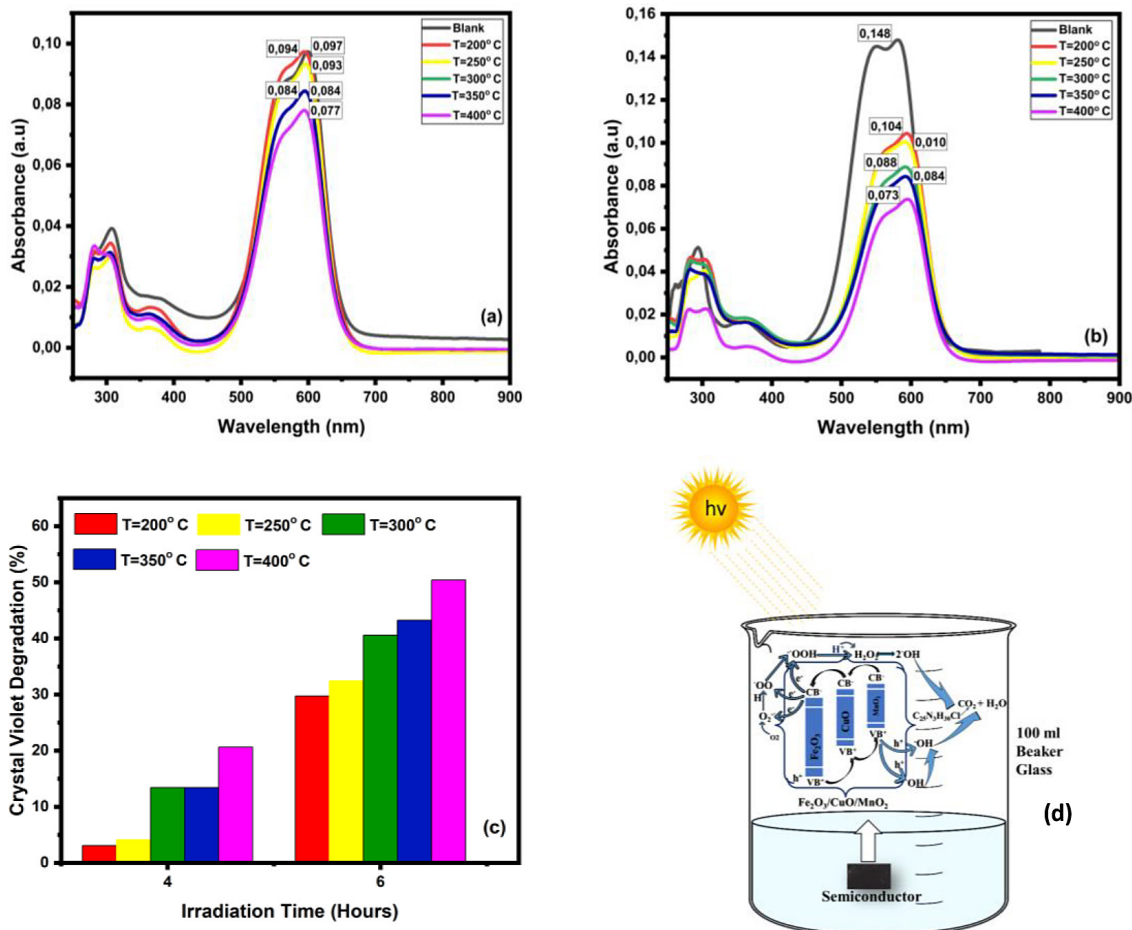
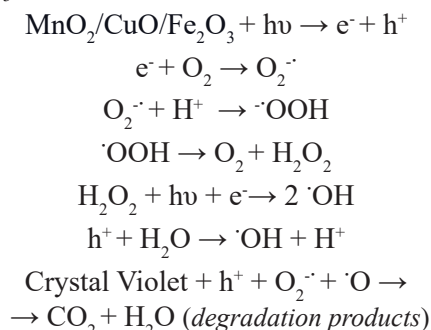


Figure 5. (a) The absorbance spectra and percentage degradation of crystal violet after (a) 4 hours and (b) 6 hours (c) % degradation after irradiation (d) mechanism of photocatalyst degradation of crystal violet

impurities. At a temperature of 400°C for 6 hours of irradiation, the optimum degradation percentage was 50.4%. The photocatalyst process shown in Figure 5 (d) determined the % degradation of the nanocomposite photocatalyst MnO₂/CuO/Fe₂O₃ in a crystal violet solution.



The MnO₂/CuO/Fe₂O₃ catalyst was illuminated by sunlight so that electron transfer occurs, resulting in reduced impurities. The photocatalyst activity of the MnO₂, CuO, and Fe₂O₃ semiconductor alloys was superior to that of single semiconductors CuO and Fe₂O₃. Photocatalyst reactions take place on the surface of alloy semiconductor materials with the assistance of sunlight. The semiconductors utilized were made from local iron ore and copper rock, which were ground into micro particles Fe₂O₃/CuO. When exposed to UV light, this alloy readily produces hole electron pairs in the conduction and valence bands. These electrons and holes contribute to the formation of free radicals in water, which then degrade organic contaminants into non-toxic molecules (Sukma et al., 2019; Ratnawulan et al., 2021). However, issues with the manufacturing of this artificial photocatalyst have been discovered, notably that the energy band gap was significant enough that photocatalyst activity was confined to the usage of sunlight in ultraviolet areas, where availability in sunlight is just 10%. As a result, we were presently attempting to combine with another semiconductor material, MnO₂, which has an energy band gap of ~1 eV. This energy band gap has consequences for light, which may be exploited to generate electrons and holes. This method was predicted to decrease the energy band gap, allowing photocatalyst activity to operate on visible light, which is plentiful.

The (e⁻) and (h⁺) recombination can be slowed down due to the charge transfer between h⁺ on Fe₂O₃ to CuO and e⁻ on CuO, which were transferred to Fe₂O₃, and vice versa with MnO₂ doping. Electrons transfer occurs from the conduction band (CB) of MnO₂ to the conduction band (CB) of CuO, and finally to the conduction band

(CB) of Fe₂O₃. Meanwhile, the photogenerated holes migrate from Fe₂O₃ to CuO, and MnO₂ in the opposite direction from the Valence Band (VB). Thus, more electrons accumulate in the CB than in Fe₂O₃. The more electrons accumulated the more impurities were reduced. The process of combining MnO₂, CuO, and Fe₂O₃ can cause the transfer of (e⁻) and (h⁺) from one semiconductor to another to reduce the band gap of CuO and MnO₂ energy. The absorption of light will shift towards infrared light. MnO₂/CuO/Fe₂O₃ accepts electrons from molecules in the surrounding media.

The mechanism of crystal violet degradation on the surface of MnO₂/CuO/Fe₂O₃ starts with photon absorption above the band gap energy of 1.36 eV, resulting in electron pairs e⁻ and h⁺. When e⁻ CB was excited or moved to fill the gap in the conduction band. It was occupied by an empty hole (h⁺ vb) that was trapped on the surface of MnO₂/CuO/Fe₂O and reacted to adsorbed substances like water, hydroxide ions, impurities crystal violet, and oxygen. On the external surface, e⁻ CB and h⁺ VB participated in redox processes involving adsorbed substances at the surface. The reaction of H₂O/OH⁻ by h⁺ VB produces OH, a highly strong oxide.

A thin layer of MnO₂/CuO/Fe₂O₃ can reduce resource consumption, permit the catalyst to remain active for an extended time and impact the environment (Becker et al., 2019; Chen et al., 2018). However, thin-layer catalysts have in that they are prone to abrasion and need expensive equipment, which can raise production costs and limitations in precisely controlling film thickness (Abid et al., 2022). The thin layer has a more homogenous surface in this application because the catalyst may degrade chemical compounds in wastewater, making it more ecologically friendly (Neeti et al., 2023). The usage of local materials was highly helpful in this study because it includes numerous impurity atoms and was predicted to lower the energy bandgap's width, allowing the final alloy to absorb all spectrums of sunlight. This study was predicted to have significant consequences since it can capture or purify water very inexpensively and easily. The photocatalyst material works with the aid of sunlight spread across the surface of the polluted water, no energy is required, and the water will be free of organic pollutants. Furthermore, the catalyst may clear debris on the surface automatically with the assistance of sunlight, within 6 hours of self-cleaning service.

CONCLUSION

A thin layer of $\text{MnO}_2/\text{CuO}/\text{Fe}_2\text{O}_3$ was successfully synthesized using the sol-gel and spin-coated technique. This layer has an energy gap between 1.36–1.67 eV, allowing it to exhibit strong photocatalytic activity. It has the potential to degrade organic pollution in crystal violet pollutants using solar energy in a wider spectrum, from ultraviolet to infrared. The optimum percentage degradation was produced by samples sintered at 400°C at 50.4% under irradiation with sunlight for six hours. This catalyst promotes photochemical reactions that result in the long-term breakdown of organic pollutants in wastewater.

Acknowledgments

The authors extend their gratitude to the Directorate General of Higher Education (DIKTI), Ministry of Research, Technology and Higher Education, Indonesia, for the research grant (Penelitian Dasar Kompetitif Nasional, 2022), No. 093/ES/PG.02.00.PT/2022.

REFERENCES

- Abid, N., Khan, A. M., Shujait, S., Chaudhary, K., Ikram, M., Imran, M., Haider, J., Khan, M., Khan, Q., & Maqbool, M. (2022). Synthesis of nanomaterials using various top-down and bottom-up approaches, influencing factors, advantages, and disadvantages: A review. *Advances in Colloid and Interface Science*, 300(December 2021), 102597. <https://doi.org/10.1016/j.cis.2021.102597>
- Alagiri, M., & Hamid, S.B.A. (2015). Sol-gel synthesis of $\alpha\text{-Fe}_2\text{O}_3$ nanoparticles and its photocatalytic application. *Journal of Sol-Gel Science and Technology*, 74(3), 783–789. <https://doi.org/10.1007/s10971-015-3663-y>
- Alp, E., Halil, E., Kür, M., & Genç, A. (2019). Synergistic activity enhancement in 2D $\text{CuO}/\text{Fe}_2\text{O}_3$ nanocomposites for the photodegradation of rhodamine B. *Ceramics International*, 45, 9174–9178. <https://doi.org/10.1016/j.ceramint.2019.01.258>
- Amin, N.H., Ali, L.I., El-molla, S.A., Ebrahim, A.A., & Mahmoud, H.R. (2016). Effect of Fe_2O_3 precursors on physicochemical and catalytic properties of $\text{CuO}/\text{Fe}_2\text{O}_3$ system. *Arabian Journal of Chemistry*, 9, S678–S684. <https://doi.org/10.1016/j.arabjc.2011.07.026>
- Ani, I.J., Akpan, U.G., Olutoye, M.A., & Hameed, B.H. (2018). Photocatalytic degradation of pollutants in petroleum refinery wastewater by TiO_2 and ZnO-based photocatalysts : Recent development. *Journal of Cleaner Production*, 205, 930–954. <https://doi.org/10.1016/j.jclepro.2018.08.189>
- Anisa, K., Ratnawulan, R., Fauzi, A., Rahmadhani, D., Steven, A., & Azleen, F. (2023). Effect of Temperature Variation on Band Gap Value in Thin Layers of Nano Photocatalyst $\text{Fe}_2\text{O}_3/\text{CuO}/\text{MnO}_2$. *IOP Conf. Series: Earth and Environmental Science*, 1228(012037). <https://doi.org/10.1088/1755-1315/1228/1/012037>
- Aroob, S., Carabineiro, S.A.C., Taj, M.B., Bibi, I., Raheel, A., Javed, T., Yahya, R., Alelwani, W., Verpoort, F., Kamwilaisak, K., Al-Farraj, S., & Sillanpää, M. (2023). Green Synthesis and Photocatalytic Dye Degradation Activity of CuO Nanoparticles. *Catalysts*, 13(3), 502. <https://doi.org/10.3390/catal13030502>
- Azleen, F., Ratnawulan, R., Fauzi, A., Rahmadhani, D., Steven, A., & Anisa, K. (2023). Effect of Composition Variation on The Crystal Size and Band Gap of Thin Film Nano Photocatalyst $\text{Fe}_2\text{O}_3/\text{CuO}/\text{MnO}_2$. *IOP Conference Series: Earth and Environmental Science*, 1228(1), 012017. <https://doi.org/10.1088/1755-1315/1228/1/012017>
- Becker, H., Güttel, R., & Turek, T. (2019). Performance of diffusion-optimized Fischer-Tropsch catalyst layers in microchannel reactors at integral operation. *Catalysis Science and Technology*, 9(9), 2180–2195. <https://doi.org/10.1039/c9cy00457b>
- Chen, H., You, S., Ma, Y., Zhang, C., Jing, B., Cai, Z., Tang, B., Ren, N., & Zou, J. (2018). Carbon Thin-Layer-Protected Active Sites for ZIF-8-Derived Nitrogen-Enriched Carbon Frameworks/Expanded Graphite as Metal-Free Catalysts for Oxygen Reduction in Acidic Media. *Chemistry of Materials*, 30(17), 6014–6025. <https://doi.org/10.1021/acs.chemmater.8b02275>
- Chiam, S.L., Pung, S.Y., & Yeoh, F.Y. (2020). Recent developments in MnO_2 -based photocatalysts for organic dye removal: a review. In *Environmental Science and Pollution Research* (Vol. 27, Issue 6, pp. 5759–5778). Springer. <https://doi.org/10.1007/s11356-019-07568-8>
- Fardood, S.T., Moradnia, F., & Ramazani, A. (2019). Green synthesis and characterization of ZnMn_2O_4 nanoparticles for photocatalytic degradation of Congo red dye and kinetic study. *Micro & Nano Letters*, 14, 986–991. <https://doi.org/10.1049/mnl.2019.0071>
- Fufa, T.O., Mengesha, A.T., & Yadav, O.P. (2014). Synthesis, Characterization and Photocatalytic Activity of $\text{MnO}_2/\text{Al}_2\text{O}_3/\text{Fe}_2\text{O}_3$ Nanocomposite For Phenol Degradation. *Chemistry and Materials Research*, 6(10), 73–87.
- Gayatri, R., Agustina, T.E., Bahrin, D., Moeksin, R., & Gustini, G. (2021). Preparation and Characterization of ZnO -Zeolite Nanocomposite for Photocatalytic Degradation by Ultraviolet Light. *Journal of Ecological Engineering*, 22(2), 178–186. <https://doi.org/10.12911/22998993/131031>

15. Karimi, R., Yousefi, F., Ghaedi, M., & Rezaee, Z. (2019). Comparison of the behavior of ZnO – NP – AC and Na, K doped ZnO – NP – AC for simultaneous removal of Crystal Violet and Quinoline Yellow dyes : Modeling and optimization. *Polyhedron*, 170, 60–69. <https://doi.org/10.1016/j.poly.2019.05.038>
16. Le, V.T., Doan, V.D., Le, T.T.N., Dao, M.U., Vo, T.T.T., Do, H.H., Viet, D.Q., & Tran, V.A. (2021). Efficient photocatalytic degradation of crystal violet under natural sunlight using Fe₃O₄/ZnO nanoparticles embedded carboxylate-rich carbon. *Materials Letters*, 283, 128749. <https://doi.org/10.1016/j.matlet.2020.128749>
17. Liu, J., Wu, P., Yang, S., Rehman, S., Ahmed, Z., Zhu, N., Dang, Z., & Liu, Z. (2020). Applied Catalysis B : Environmental A photo-switch for peroxydisulfate non-radical/radical activation over layered CuFe oxide: Rational degradation pathway choice for pollutants. *Catalysis*, 261, 118232. <https://doi.org/10.1016/j.apcatb.2019.118232>
18. Mamiyev, Z., & Balayeva, N.O. (2022). Metal Sulfide Photocatalysts for Hydrogen Generation: A Review of Recent Advances. *Catalysts*, 12, 1–36. <https://doi.org/https://doi.org/10.3390/catal12111316> Academic
19. Mandrekar, P.P., & D'souza, A. (2023). Green Synthesis of Copper Oxide Nanoparticles Using Coffe, Piper Nigrum, and Coriandrum Sativum and its Application in Photocatalytic Degradation of Methylene Blue Dye. *Rasayan Journal of Chemistry*, 16(1), 276–283. <https://doi.org/10.31788/RJC.2023.1616889>
20. Mesrar, M., Elbasset, A., Mrabet, I. El, Zaitan, H., Abdi, F., Echatoui, N., & Lamcharfi, T. (2023). Hydrothermal Synthesis and Characterization of Sodium Bismuth Titanate for Photocatalytic Applications. *Journal of Ecological Engineering*, 24(10), 185–197.
21. Mondal, D., Das, S., Kumar, B., & Bhattacharya, D. (2019). Size-engineered Cu-doped α -MnO₂ nanoparticles for exaggerated photocatalytic activity and energy storage application. *Materials Research Bulletin*, 115, 159–169. <https://doi.org/10.1016/j.materresbull.2019.03.023>
22. Neeti, K., Singh, R., & Ahmad, S. (2023). The role of green nanomaterials as effective adsorbents and applications in wastewater treatment. *Materials Today: Proceedings*, 77, 269–276. <https://doi.org/10.1016/j.matpr.2022.11.300>
23. Pawar, S.A., Patil, D.S., & Shin, J.C. (2019). Transition of hexagonal to square sheets of Co₃O₄ in a triple heterostructure of Co₃O₄/MnO₂/GO for high-performance supercapacitor electrode. *Current Applied Physics*, 19(7), 794–803. <https://doi.org/10.1016/j.cap.2019.04.009>
24. Permana, M.D., Noviyanti, A.R., Lestari, P.R., Kumada, N., Eddy, D.R., & Rahayu, I. (2022). Enhancing the Photocatalytic Activity of TiO₂/Na-2Ti₆O₁₃ Composites by Gold for the Photodegradation of Phenol. *Chemengineering*, 6(5). <https://doi.org/10.3390/chemengineering6050069>
25. Ratnawulan, R., Ramli, R., Fauzi, A., & Sukma Hayati, A.E. (2021). Synthesis and characterization of polystyrene/Cuo-Fe₂O₃ nanocomposites from natural materials as hydrophobic photocatalytic coatings. *Crystals*, 11(1), 1–13. <https://doi.org/10.3390/cryst11010031>
26. Ratnawulan, R., Sarimai, S., & Fauzi, A. (2022). The Synthesis of CuO/ Polystyrene Nanocomposite Superhydrophobic Layer using The Spin Coating Method. *Science and Technology Indonesia*, 7(2), 158–163. <https://doi.org/https://doi.org/10.26554/sti.2022.7.2.158-163>
27. Sukma, H., Ratnawulan, R., & Ramli, R. (2019). Semiconductor-Based Photocatalysts Degradation of Methyl Orange Using Cuo-Fe₂O₃ Nanocomposites. *International Journal of Progressive Sciences and Technologies (IJPSAT)*, 15(1), 1–5.
28. Surendra, B.S., Veerabhadrswamy, M., Anantharaju, K.S., Nagaswarupa, H.P., & Prashantha, S.C. (2018). Green and chemical-engineered CuFe₂O₄ characterization cyclic voltammetry, photocatalytic and photoluminescent investigation for multifunctional applications. *Journal of Nanostructure in Chemistry*, 8, 45–59. <https://doi.org/http://doi.org/10.1007/s40097-018-0253-x>
29. Touqeer, M., Baig, M.M., Aadil, M., Philips, O., Shakir, I., Aboud, M.F.A., & Warsi, M.F. (2020). New Co-MnO based Nanocrystallite for photocatalysis studies driven by visible light. *Journal of Taibah University for Science*, 14(1), 1580–1589. <https://doi.org/10.1080/16583655.2020.1846966>
30. Wadi, K. M., Jasim, K. A., Shaban, A. H., Kamil, M. K., & Nsaif, F. K. (2020). The effects of sustainable manufacturing pressure on the structural properties of the pb2ba2ca2cu3o9+ σ compound. *Journal of Green Engineering*, 10(9), 6052–6062.
31. Wang, Y., Silveri, F., Bayazit, M. K., Ruan, Q., Li, Y., Xie, J., Catlow, C.R.A., & Tang, J. (2018). Bandgap Engineering of Organic Semiconductors for Highly Efficient Photocatalytic Water Splitting. *Advance Energy Material*, 8, 1801084. <https://doi.org/10.1002/aenm.201801084>
32. Yuniar, Agustina, T. E., Faizal, M., & Hariani, P. L. (2023). Synthesis and Characterization of ZnO/Mn-Fe₂O₄ Nanocomposites for Degrading Cationic Dyes. *Journal of Ecological Engineering*, 24(4), 252–263. <https://doi.org/10.12911/22998993/160514>
33. Zhang, Y., Liu, L., Chen, Y., Cheng, X., Song, C., Ding, M., & Zhao, H. (2019). Synthesis of MnO₂-CuO-Fe₂O₃/CNTs catalysts: Low-temperature SCR activity and formation mechanism. *Beilstein Journal of Nanotechnology*, 10, 848–855. <https://doi.org/10.3762/BJNANO.10.85>